# Second-order Synchrosqueezing Transform: The Wavelet Case, Comparisons and Applications

Duong-Hung Pham, Sylvain Meignen

# Second-order Synchrosqueezing Transform: The Wavelet Case, Comparisons and Applications

Duong-Hung Pham[1], and Sylvain Meignen[2]
[1,2]Jean Kuntzmann Laboratory- Bâtiment IMAG,
Université Grenoble Alpes
700 Avenue Centrale
Campus de Saint Martin d'Hères
38401 Domaine Universitaire de Saint-Martin-d'Hères.

**Abstract**

This paper addresses the analysis of the time-frequency technique so-called the second-order synchrosqueezing transform derived from continuous wavelet transform of multicomponent AM-FM signals. Such a technique is designed to deal with signals consisting of components (or modes) with strong frequency modulation . Before going into the details of this analysis, we revisit the case where the modes are assumed to be with weak frequency modulation as in the seminal paper of Daubechies et *al.* [1], but not assuming the wavelet is compactly supported in the Fourier domain. The remainder of the paper is devoted to the theoretical analysis of the second order wavelet-based synchrosqueezing transform and to numerical simulations emphasizing the differences between this new synchrosqueezing transform and existing ones. An illustration of the benefits of using this new synchrosqueezing operator for the analysis of gravitational wave concludes the paper.

*Keywords:* Time-frequency analysis, reassignment, synchrosqueezing, AM/FM, multicomponent signals.

## 1. Introduction

Many signals arising from audio recordings (music, speech), meteorology, structural stability analysis [2, 3, 4], or medical data (electrocardiogram, thoracic and abdominal movement signals) [5, 6], can be modeled as a sum of amplitude- and frequency-modulated (AM-FM) modes, called multicomponent

[1]Email:duong-hung.pham@univ-grenoble-alpes.fr
[2]Email:sylvain.meignen@univ-grenoble-alpes.fr

signals (MCS) [7]. Time-frequency (TF) analysis plays a central role for characterizing such signals and, in that framework, numerous methods have been developed for the last two decades. Standard linear methods, as for instance the short-time Fourier transform (STFT) and the continuous wavelet transform (CWT), have been the most commonly used [8]. However, the effectiveness of each method strongly depends on the nature of the modes constituting the signal and is limited by the trade-off between time and frequency resolution known as *uncertainty principle*. Several attempts were made to overcome this shortcoming and one of them, called the *reassignment method* (RM), received a considerable attention. The concept of RM dates back to Kodera et *al.* [9] in the 1970's and was further developed in [10], where it was viewed as a means of improving the readability of TF representations. Unfortunately, RM suffers from an inherent limitation which is its non invertibility, namely it does not allow for mode reconstruction.

In an independent work [1], Daubechies et *al.* introduced an adaptive wavelet-based signal analysis method known as the *synchrosqueezing transform* (WSST), an adaptation of RM enabling modes' retrieval. An extension of WSST to the TF representation given by STFT, called *STFT-based synchrosqueezing transform* (FSST), was proposed in [11], while efforts were put on exploring the bidimensional case, as for instance by using the monogenic synchrosqueezed wavelet transform [12], developing other types of TF representations as the synchrosqueezed wavelet packet transform [13, 14], or multi-taper approaches as in the ConceFT technique [15]. In spite of all these advances, one major problem associated with synchrosqueezing techniques, in their original formulation, is that they cannot deal with MCS containing modes with strong frequency modulation, very common in many fields of practical interest, as for instance chirps involved in radar [16], speech processing [17], or gravitational waves [18, 19]. In this regard, an adaptation of FSST to better handle that type of signals, known as the *second order synchrosqueezing transform* (FSST2), was introduced in [20] and its theoretical foundations settled in [21].

In the present paper, our goal is to build up a second order extension of WSST for which we develop a mathematical analysis and discuss its practical implementation. To do so, after having recalled some useful definitions in Section 2, we revisit WSST assuming the analysis wavelet is not compactly supported in the Fourier domain, in Section 3. This helps derive, in Section 4, the second order wavelet-based synchrosqueezing transform (WSST2) and then prove approximations results generalizing those related to WSST. In Section 5, we detail the practical implementation of WSST2, and carry out numerical experiments to compare, on simulated and real signals, the proposed approach with existing synchrosqueezing transforms, in Section 6.

## 2. Background

Before going in detail into the principle of WSST, we recall useful notation and definitions.

The Fourier transform (FT) of a given signal $f \in L^1(\mathbb{R})$ is defined as:

$$\widehat{f}(\eta) = \mathcal{F}\{f\}(\eta) = \int_{\mathbb{R}} f(t) e^{-i2\pi\eta t} dt. \tag{1}$$

Let us consider a wavelet $\psi \in L^1(\mathbb{R})$ and a signal $f \in L^\infty(\mathbb{R})$, and then define for any time $t$ and scale $a > 0$, the *continuous wavelet transform* (CWT) of $f$ by:

$$W_f^\psi(t,a) = \frac{1}{a} \int_{\mathbb{R}} f(\tau) \overline{\psi\left(\frac{\tau - t}{a}\right)} d\tau, \tag{2}$$

where $\overline{Z}$ denotes the complex conjugate of $Z$. If $f$ and $\hat{f}$ are in $L^1(\mathbb{R})$ and $f$ is continuous and analytic, i.e. $\hat{f}(\eta) = 0$ if $\eta < 0$, and assuming $C'_\psi = \int_0^{+\infty} \overline{\widehat{\psi}(\eta)} \frac{d\eta}{\eta} < \infty$, one has the following reconstruction formula:

$$f(t) = \frac{1}{C'_\psi} \int_0^{+\infty} W_f^\psi(t,a) \frac{da}{a}. \tag{3}$$

In this paper, we will intensively study multicomponent signals (MCS) defined as a superposition of AM-FM components or modes:

$$f(t) = \sum_{k=1}^{K} f_k(t) \quad \textit{with} \quad f_k(t) = A_k(t) e^{i2\pi\phi_k(t)}, \tag{4}$$

for some finite $K \in \mathbb{N}$, $A_k(t)$ and $\phi'_k(t)$ are respectively instantaneous amplitude (IA) and frequency (IF) of mode $f_k$ satisfying: $A_k(t) > 0, \phi'_k(t) > 0$ and $\phi'_{k+1}(t) > \phi'_k(t)$ for all $t$. Such a signal is fully described by its ideal TF (ITF) representation defined as:

$$\mathrm{TI}_f(t,\omega) = \sum_{k=1}^{K} A_k(t) \delta\left(\omega - \phi'_k(t)\right), \tag{5}$$

where $\delta$ denotes the Dirac distribution.

## 3. Wavelet-based synchrosqueezing transform (WSST)

### *3.1. WSST principle*

The wavelet-based SST (WSST) was originally introduced in the context of auditory signal analysis [22] and further studied mathematically in [1]. Its

principle is to sharpen the "blurred" representation given by the CWT by using the following IF estimate at time $t$ and scale $a$:

$$\widehat{\omega}_f(t,a) = \Re\left\{\frac{1}{i2\pi}\frac{\partial_t W_f^\psi(t,a)}{W_f^\psi(t,a)}\right\}, \tag{6}$$

where $\Re\{Z\}$ stands for the real part of complex number $Z$ and $\partial_t$ is the partial derivative with respect to $t$.

Indeed, $W_f^\psi(t,a)$ is reassigned to a new position $(t, \widehat{\omega}_f(t,a))$ using the synchrosqueezing operator defining WSST, as follows:

$$S^\gamma_{W_f^\psi}(t,\omega) = \int_{|W_f^\psi(t,a)|>\gamma} W_f^\psi(t,a)\delta\left(\omega - \widehat{\omega}_f(t,a)\right)\frac{da}{a}, \tag{7}$$

with $\gamma$ some threshold parameter.

Since the coefficients of CWT are reassigned along the "scale" axis, WSST preserves the causality property, thus making the $k^{th}$ mode approximately reconstructed by integrating $S^\gamma_{W_f^\psi}(t,\omega)$ in the vicinity of the corresponding ridge $(t, \frac{1}{\phi_k'(t)})$ in the time-scale (TS) plane:

$$f_k(t) \approx \frac{1}{C'_\psi}\int_{\{\omega,|\omega-\varphi_k(t)|<d\}} S^\gamma_{W_f^\psi}(t,\omega)d\omega, \tag{8}$$

where $\varphi_k(t)$ is an estimate of $\phi_k'(t)$, which is often computed by a ridge extraction technique [23, 24]. Parameter $d$ enables to compensate for both the inaccurate approximation $\varphi_k(t)$ of $\phi_k'(t)$ and the error made by estimating the IF by means of $\widehat{\omega}_f(t,a)$.

### *3.2. WSST mathematical framework*

WSST is supported by a solid mathematical framework [1], which we now recall. Let us first define the class of chirp-like functions (signals) on which one builds the theory:

**Definition 1.** *Let $\varepsilon > 0$ and $c > 0$. The set $\mathcal{A}_{c,\varepsilon}$ of multicomponent signals with modulation $\varepsilon$ and separation $c$ corresponds to signals defined in (4) with $f_k$ satisfying:*

$$\begin{gathered} A_k \in C^1(\mathbb{R}) \cap L^1(\mathbb{R}) \cap L^\infty(\mathbb{R}), \phi_k \in C^2(\mathbb{R}), \\ \inf_{t\in\mathbb{R}} \phi_k'(t) > 0, \sup_{t\in\mathbb{R}} \phi_k'(t) < \infty, M = \max_k\left(\sup_{t\in\mathbb{R}} \phi_k'(t)\right), \\ A_k(t) > 0, |A_k'(t)| \le \varepsilon\phi_k'(t) \le \varepsilon M, |\phi_k''(t)| \le \varepsilon\phi_k'(t) \le \varepsilon M, \quad \forall t \in \mathbb{R}. \end{gathered}$$

*Further, the $f_k$s are separated with resolution $c$, i.e., for all $k \in \{1,\dots,K-1\}$ and all $t$*

$$\phi_{k+1}'(t) - \phi_k'(t) \ge c(\phi_{k+1}'(t) + \phi_k'(t)). \tag{9}$$

In what follows $\Delta$ denotes a real number in $]0, \frac{c}{c+1}[$.

**Definition 2.** *Let $h$ be a positive $L^1$-normed window belonging to $C_0^\infty(\mathbb{R})$, the set of compactly supported $C^\infty$ functions on $\mathbb{R}$, and consider $\gamma, \lambda > 0$. The wavelet-based synchrosqueezing transform of $f$ (WSST) with threshold $\gamma$ and accuracy $\lambda$ is defined by:*

$$S^{\lambda,\gamma}_{W_f^\psi}(t,\omega) := \int_{|W_f^\psi(t,a)|>\gamma} W_f^\psi(t,a)\frac{1}{\lambda}h\left(\frac{\omega - \widehat{\omega}_f(t,a)}{\lambda}\right)\frac{da}{a}. \tag{10}$$

*If $\lambda \to 0$, then $S^{\lambda,\gamma}_{W_f^\psi}(t,\omega)$ tends, in the sense of distribution, to some value which we formally write as in (7).*

**Theorem 1.** *Consider $f \in \mathcal{A}_{c,\varepsilon}$, set $\widetilde{\varepsilon} = \varepsilon^{\frac{1}{3}}$ and let $\psi$ be a non-compactly supported wavelet in the Fourier domain satisfying: $\left|\hat{\psi}(\eta)\right| \leq N_0\varepsilon$ when $|\eta - 1| > \Delta$, and $\int_{|\eta-1|>\Delta}\left|\hat{\psi}(\eta)\right|\frac{d\eta}{\eta} \leq N_1\widetilde{\varepsilon}$, for some constants $N_0$ and $N_1$.*

*Assuming $(t,a) \in \mathbb{E} = \mathbb{R} \times \left[0, \frac{1+\Delta}{\inf_{t\in\mathbb{R}}\phi_1'(t)}\right]$, then, provided $\varepsilon$ is sufficiently small, the following hold:*

- *(a) $|W_f^\psi(t,a)| > \widetilde{\varepsilon}$ only when, there exists $k \in \{1,\dots,K\}$, such that $(t,a) \in Z_k := \{(t,a),\ s.t.\ |a\phi_k'(t) - 1| < \Delta\}$.*
- *(b) For each $k \in \{1,\dots,K\}$ and all $(t,a) \in Z_k$ for which holds $|W_f^\psi(t,a)| > \widetilde{\varepsilon}$, one has:*

$$|\widehat{\omega}_f(t,a) - \phi_k'(t)| \leq \widetilde{\varepsilon}. \tag{11}$$

- *(c) Moreover, for each $k \in \{1,\dots,K\}$, there exists a constant $D_1$ such that for any $t \in \mathbb{R}$*

$$\left|\lim_{\lambda\to 0}\left(\frac{1}{C'_\psi}\int_{|\omega-\phi_k'(t)|<\widetilde{\varepsilon}} S^{\lambda,\widetilde{\varepsilon}}_{W_f^\psi}(t,\omega)d\omega\right) - f_k(t)\right| \leq D_1\widetilde{\varepsilon}. \tag{12}$$

It is worth noting that WSST framework for a compactly supported wavelet in the Fourier domain was already studied in [1]. It is however useful for real-time applications [25] to extend this result to non compact wavelet in the Fourier domain framework as is illustrated by Theorem 1.

The main steps for the proof of the latter are detailed hereafter. First, we introduce the following proposition that is useful to prove item (a) of Theorem 1.

**Proposition 1.** *For any $(t,a) \in \mathbb{R} \times \mathbb{R}^+$, one has:*

$$\left|W_f^\psi(t,a) - \sum_{k=1}^{K} f_k(t)\overline{\hat{\psi}(a\phi_k'(t))}\right| \leq \varepsilon E_0(t,a), \tag{13}$$

*where* $E_p(t,a) = aMKJ_{1,p} + \pi a^2 MJ_{2,p} \sum_{k=1}^{K} A_k(t)$ *and* $J_{n,p} = \int_{\mathbb{R}} |u|^n |\psi^{(p)}(u)| du$.

The proof of Proposition 1 is available in Section Appendix A1.

Now we can prove item (a) of Theorem 1: since $E_0(t,a)$ is bounded on $\mathbb{E}$, we can consider:

$$\widetilde{\varepsilon} \leq \frac{1}{\sqrt{2}} \min \left( \|E_0(t,a)\|_{\infty,\mathbb{E}}^{-\frac{1}{2}}, \left\| N_0 \sum_{k=1}^{K} A_k(t) \right\|_{\infty,\mathbb{E}}^{-\frac{1}{2}} \right) \tag{14}$$

where $\|z(t,a)\|_{\infty,X} = \sup_{(t,a)\in X} |z(t,a)|$. For $(t,a) \in \mathbb{E} \setminus \bigcup_{l=1}^{K} Z_l$, we immediately get $|W_f^{\psi}(t,a)| \leq \widetilde{\varepsilon}$. Thus, if $|W_f^{\psi}(t,a)| > \widetilde{\varepsilon}$, there is at least one $k$ such that $(t,a) \in Z_k$. Furthermore, because of the separation condition on the modes, one can easily show the $Z_k$s are disjoint sets, so $k$ is unique.

**Remark 1.** Note that $E_0(t,a)$ is uniformly bounded for $(t,a) \in \mathbb{E}$ because $a$ is lower than $\alpha$. In the seminal paper of Daubechies [1], this constraint on $a$ was missing.

Let us now detail the proof of item (b) of Theorem 1. Writing Proposition 1 with wavelet $\psi'$ we get for any $(t,a) \in \mathbb{R} \times \mathbb{R}^+$:

$$\left| W_f^{\psi'}(t,a) + \sum_{k=1}^{K} f_k(t) 2i\pi a \phi_k'(t) \overline{\hat{\psi}(a\phi_k'(t))} \right| \leq \varepsilon E_1(t,a),$$

with $E_1(t,a)$ being defined at the end of Proposition 1. Thus, if $(t,a) \in Z_k$, one gets:

$$\left| W_f^{\psi'}(t,a) + f_k(t) 2i\pi a \phi_k'(t) \overline{\hat{\psi}(a\phi_k'(t))} \right| \leq \varepsilon \left( 2\pi N_0 a \sum_{l \neq k} \phi_l'(t) A_l(t) + E_1(t,a) \right).$$

Note that since $\partial_t W_f^{\psi}(t,a) = -\frac{1}{a} W_f^{\psi'}(t,a)$, one can right for $(t,a) \in Z_k$

satisfying $|W_f^\psi(t,a)| > \widetilde{\varepsilon}$:

$$
\begin{aligned}
|\widehat{\omega}_f(t,a) - \phi_k'(t)| &= \left| \Re\left\{ \frac{1}{2\pi} \frac{\partial_t W_f^\psi(t,a)}{W_f^\psi(t,a)} - \phi_k'(t) \right\} \right| \\
&= \left| \Re\left\{ \frac{1}{i2\pi a} \frac{W_f^{\psi'}(t,a) + i2\pi a \phi_k'(t) W_f^\psi(t,a)}{W_f^\psi(t,a)} \right\} \right| \\
\leq \left| \frac{1}{i2\pi a} \frac{W_f^{\psi'}(t,a) + 2i\pi a \phi_k'(t) f_k(t) \overline{\hat{\psi}(a\phi_k'(t))}}{W_f^\psi(t,a)} \right| &+ \left| \frac{\phi_k'(t) W_f^\psi(t,a) - \phi_k'(t) f_k(t) \overline{\hat{\psi}(a\phi_k'(t))}}{W_f^\psi(t,a)} \right| \\
&\leq \widetilde{\varepsilon}^2 \left( N_0 \sum_{l \neq k} (\phi_l'(t) + \phi_k'(t)) A_l(t) + \frac{E_1(t,a)}{2\pi a} + \phi_k'(t) E_0(t,a) \right).
\end{aligned}
$$

By putting, $B_k(t,a) = N_0 \sum_{l \neq k} (\phi_l'(t) + \phi_k'(t)) A_l(t) + \frac{E_1(t,a)}{2\pi a} + \phi_k'(t) E_0(t,a)$, and remarking it is bounded on $\mathbb{E}$, we may choose :

$$
\widetilde{\varepsilon} \leq \min_k \| B_k(t,a) \|_{\infty,\mathbb{E}}^{-1}, \tag{15}
$$

so that for $(t,a) \in Z_k$ such that $|W_f^\psi(t,a)| > \widetilde{\varepsilon}$, we immediately get:

$$
|\widehat{\omega}_f(t,a) - \phi_k'(t)| \leq \widetilde{\varepsilon}. \tag{16}
$$

Let us now introduce the following lemma, which is useful to prove item (c) of Theorem 1.

**Lemma 1.** *Suppose that both (14) and (15) are satisfied, and that the following condition is also verified:*

$$
\varepsilon \leq 1/8c^3 (\phi_1'(t) + \phi_2'(t))^3. \tag{17}
$$

*Consider the following sets:*

$$
\begin{aligned}
\mathbb{X} &= \{ a \ s.t. \ |W_f^\psi(t,a)| > \widetilde{\varepsilon} \ and \ |\widehat{\omega}_f(t,a) - \phi_k'(t)| \leq \widetilde{\varepsilon} \}, \\
\mathbb{Y} &= \{ a \ s.t. \ |W_f^\psi(t,a)| > \widetilde{\varepsilon} \ and \ |a\phi_k'(t) - 1| < \Delta \},
\end{aligned}
$$

*then* $\mathbb{X} = \mathbb{Y}$.

The proof of Lemma 1 is available in available in [1] .

Coming back to the proof of item (c) of Theorem 1, let $t \in \mathbb{R}$ and note that $W_f^\psi(t,a) \in L^\infty(\mathbb{X})$. Then, since $a > 0$ on $\mathbb{X}$, $\frac{1}{a} W_f^\psi(t,a) \in L^1(\mathbb{X})$, and, thus,

using the same type of technique as in [1] (Estimate 3.9), one gets:

$$\left|\lim_{\lambda\to 0}\left(\frac{1}{C'_\psi}\int_{|\omega-\phi'_k(t)|<\widetilde{\varepsilon}} S^{\lambda,\widetilde{\varepsilon}}_{W^\psi_f}(t,\omega)d\omega\right)-f_k(t)\right| = \left|\frac{1}{C'_\psi}\int_{\mathbb{X}} W^\psi_f(t,a)\frac{da}{a}-f_k(t)\right|$$

$$\leq \left|\frac{1}{C'_\psi}\int_{|a\phi'_k(t)-1|<\Delta} W^\psi_f(t,a)\frac{da}{a}-f_k(t)\right| + \left|\frac{1}{C'_\psi}\int_{|W^\psi_f(t,a)|\leq\widetilde{\varepsilon}\cap|a\phi'_k(t)-1|<\Delta} W^\psi_f(t,a)\,\frac{da}{a}\right|$$

$$\leq \frac{1}{\left|C'_\psi\right|}\left[\int_{|a\phi'_k(t)-1|<\Delta}\left|W^\psi_f(t,a)-f_k(t)\overline{\hat{\psi}(a\phi'_k(t))}\right|\frac{da}{a}+\frac{A_k(t)}{\left|C'_\psi\right|}\int_{|a\phi'_k(t)-1|\geq\Delta}\left|\hat{\psi}(a\phi'_k(t))\right|\frac{da}{a}+\right.$$

$$\left.\widetilde{\varepsilon}\log\left(\frac{1+\Delta}{1-\Delta}\right)\right]$$

$$\leq \frac{1}{\left|C'_\psi\right|}\left[\int_{|a\phi'_k(t)-1|<\Delta}\varepsilon(E_0(t,a)+N_0\sum_{l\neq k}A_l(t))\frac{da}{a}+A_k(t)N_1\widetilde{\varepsilon}+\widetilde{\varepsilon}\log\left(\frac{1+\Delta}{1-\Delta}\right)\right]$$

$$\leq \widetilde{\varepsilon}\frac{1}{\left|C'_\psi\right|}\left[\|A_k\|_\infty N_1+2\log\left(\frac{1+\Delta}{1-\Delta}\right)\right]\leq D_1\widetilde{\varepsilon}$$

which ends up proving the theorem.

## 4. Second order wavelet-based SST (WSST2)

### *4.1. Second order IF estimate*

Although WSST proves to be an efficient solution to enhance TF representations, its applicability is restricted to a class of MCS composed of slightly perturbed purely harmonic modes. To overcome this limitation, a recent extension of WSST was introduced based on a more accurate IF estimate, which is then used to define an improved synchrosqueezing operator, called *second-order wavelet-based synchrosqueezing transform* (WSST2) [26], and our goal is to carry out its mathematical study.

More precisely, we first define a second-order local modulation operator, which is then used to compute the new IF estimate. This modulation operator corresponds to the ratio of the first-order derivatives, with respect to $t$, of the reassignment operators, as explained in the following:

**Proposition 2.** *Given a signal $f\in L^\infty(\mathbb{R})$, the complex reassignment operators $\widetilde{\omega}_f(t,a)$ and $\widetilde{\tau}_f(t,a)$ are respectively defined for any $(t,a)$ s.t. $W^\psi_f(t,a)\neq 0$ as:*

$$\widetilde{\omega}_f(t,a)=\frac{1}{i2\pi}\frac{\partial_t W^\psi_f(t,a)}{W^\psi_f(t,a)} \tag{18}$$

$$\widetilde{\tau}_f(t,a)=\frac{\int_{\mathbb{R}}\tau f(\tau)\frac{1}{a}\overline{\psi(\frac{\tau-t}{a})}d\tau}{W^\psi_f(t,a)}=t+a\frac{W^{t\psi}_f(t,a)}{W^\psi_f(t,a)}, \tag{19}$$

*which are defined provided $t\psi$ and $\psi'$ are in $L^1(\mathbb{R})$. Then, the second-order local complex modulation operator $\widetilde{q}_{t,f}(t,a)$ is defined by:*

$$\widetilde{q}_{t,f}(t,a) = \frac{\partial_t \widetilde{\omega}_f(t,a)}{\partial_t \widetilde{\tau}_f(t,a)}, \qquad \textit{whenever } \partial_t \widetilde{\tau}_f(t,a) \neq 0. \tag{20}$$

**Remark 2.** It is interesting to note that using partial derivatives with respect to $a$ instead of $t$, one can obtain a new second-order local modulation operator $\widetilde{q}_{a,f}(t,a) = \dfrac{\partial_a \widetilde{\omega}_f(t,a)}{\partial_a \widetilde{\tau}_f(t,a)}$, whose properties are exactly the same as those of $\widetilde{q}_{t,f}(t,a)$.

In this regard, the definition of the improved IF estimate associated with the TF representation given by CWT is derived as:

**Definition 3.** *Let $f \in L^\infty(\mathbb{R})$, the second-order local complex IF estimate of $f$ is defined as:*

$$\widetilde{\omega}_f^{[2]}(t,a) = \begin{cases} \widetilde{\omega}_f(t,a) + \widetilde{q}_{t,f}(t,a)(t - \widetilde{\tau}_f(t,a)) & \textit{if } \partial_t \widetilde{\tau}_f(t,a) \neq 0 \\ \widetilde{\omega}_f(t,a) & \textit{otherwise.} \end{cases} \tag{21}$$

*Then, its real part $\widehat{\omega}_f^{[2]}(t,a) = \Re\{\widetilde{\omega}_f^{[2]}(t,a)\}$ is the desired IF estimate.*

It was shown in [26] that $\Re\{\widetilde{q}_{t,f}(t,a)\} = \phi''(t)$ when $f$ is a Gaussian modulated linear chirp, i.e. $f(t) = A(t)e^{i2\pi\phi(t)}$ where both $\log(A(t))$ and $\phi(t)$ are quadratic. Also, $\Re\{\widetilde{\omega}_f^{[2]}(t,a)\}$ is an exact estimate of $\phi'(t)$ for this kind of signals. For a more general mode with Gaussian amplitude, its IF can be estimated by $\Re\{\widetilde{\omega}_f^{[2]}(t,a)\}$, in which the estimation error only involves the derivatives of the phase with orders larger than 3. Furthermore, $\widetilde{\omega}_f(t,a)$ and $\widetilde{q}_{t,f}(t,a)$ can be computed by means of only five CWTs as follows:

**Proposition 3.** *Let $f \in L^\infty(\mathbb{R})$, $\widetilde{\omega}_f(t,a)$ and $\widetilde{q}_{t,f}(t,a)$ can be written as:*

$$\widetilde{\omega}_f(t,a) = -\frac{1}{i2\pi a} \frac{W_f^{\psi'}(t,a)}{W_f^{\psi}(t,a)} \tag{22}$$

$$\widetilde{q}_{t,f}(t,a) = \frac{1}{i2\pi a^2} \frac{W_f^{\psi''}(t,a) W_f^{\psi}(t,a) - W_f^{\psi'}(t,a)^2}{W_f^{t\psi}(t,a) W_f^{\psi'}(t,a) - W_f^{t\psi'}(t,a) W_f^{\psi}(t,a)}, \tag{23}$$

*where $t \mapsto W^{\psi'}, W^{t\psi}, W^{\psi''}, W^{t\psi'}$ are respectively CWTs of $f$ computed with wavelets $\psi', t\psi, \psi'', t\psi'$ all in $L^1(\mathbb{R})$.*

*Proof.* These expressions are easily derived using $\partial_t^p W_f^{\psi}(t,a) = \left(-\frac{1}{a}\right)^p W_f^{\psi^{(p)}}(t,a)$. □

The second-order WSST (WSST2) is then defined by simply replacing $\widehat{\omega}_f(t,a)$ by $\widehat{\omega}_f^{[2]}(t,a)$ in (7):

$$S^{\gamma}_{2,W_f^{\psi}}(t,\omega) := \int_{|W_f^{\psi}(t,a)|>\gamma} W_f^{\psi}(t,a)\delta\left(\omega - \widehat{\omega}_f^{[2]}(t,a)\right)\frac{da}{a}, \tag{24}$$

and $f_k$ is finally retrieved by replacing $S^{\gamma}_{W_f^{\psi}}(t,\omega)$ by $S^{\gamma}_{2,W_f^{\psi}}(t,\omega)$ in (8).

### *4.2. Mathematical foundations for WSST2*

This section begins with the definition of another class of chirp-like functions, larger than $\mathcal{A}_{c,\varepsilon}$ and that can be successfully dealt with WSST2:

**Definition 4.** *Let $\varepsilon > 0$. The set $\mathcal{A}^{[2]}_{c,\varepsilon}$ of multicomponent signals with second order modulation $\varepsilon$ and separation $c$ corresponds to the signals defined in (4) satisfying:*

*(a) $f_k$ is such that $A_k$ and $\phi_k$ satisfy the following conditions:*

$$\begin{gathered}
A_k(t) \in C^2(\mathbb{R}) \cap L^1(\mathbb{R}) \cap L^{\infty}(\mathbb{R}),\ \phi_k(t) \in C^3(\mathbb{R}),\\
\phi_k'(t),\ \phi_k''(t),\ \phi_k'''(t) \in L^{\infty}(\mathbb{R}),\\
A_k(t) > 0,\ \inf_{t\in\mathbb{R}} \phi_k'(t) > 0,\ \sup_{t\in\mathbb{R}} \phi_k'(t) < \infty,\quad M = \max_k \left(\sup_{t\in\mathbb{R}} \phi_k'(t)\right),\\
|A_k'(t)| \le \varepsilon\phi_k'(t) \le \varepsilon M, |A_k''(t)| \le \varepsilon\phi_k'(t) \le \varepsilon M,\\
\text{and } |\phi_k'''(t)| \le \varepsilon\phi_k'(t) \le \varepsilon M \quad \forall t \in \mathbb{R}.
\end{gathered}$$

*(b) the $\phi_k$s satisfy the following separation condition*

$$\phi_{k+1}'(t) - \phi_k'(t) \ge c(\phi_{k+1}'(t) + \phi_k'(t)), \forall t \in \mathbb{R}\ ,\ \forall k \in \{1,\dots,K-1\}.$$

As previously mentioned, $\Delta$ is some value in $]0, \frac{c}{c+1}[$. Now, let us define WSST2 as follows:

**Definition 5.** *Let $h$ be a positive $L^1$-normed window belonging to $C_0^{\infty}(\mathbb{R})$, and consider $\gamma, \lambda > 0$, WSST2 of $f$ with threshold $\gamma$ and accuracy $\lambda$ is defined by:*

$$S^{\lambda,\gamma}_{2,W_f^{\psi}}(t,\omega) := \int_{|W_f^{\psi}(t,a)|>\gamma} W_f^{\psi}(t,a)\frac{1}{\lambda}h\left(\frac{\omega - \widehat{\omega}_f^{[2]}(t,a)}{\lambda}\right)\frac{da}{a}. \tag{25}$$

In Section 3, we showed that, for functions $f \in \mathcal{A}_{c,\varepsilon}$, a good IF estimate was given by $\widehat{\omega}_f(t,a)$ and the approximation theorem followed. Here, to assess the approximation property of WSST2 we have just introduced, we consider $f \in \mathcal{A}^{[2]}_{c,\varepsilon}$ for which we are going to prove that $\widehat{\omega}_f^{[2]}(t,a)$ is a good IF estimate. The approximation theorem is as follows:

**Theorem 2.** *Consider $f \in \mathcal{A}^{[2]}_{c,\widetilde{\varepsilon}}$, set $\widetilde{\varepsilon} = \varepsilon^{1/6}$. Let $\psi$ be a wavelet satisfying, for all $k = 1, \cdots, K$, $r \in \{0,1\}$ and $p \in \{0,1\}$, $\left|\mathcal{F}\{\tau^r \psi^{(p)}(\tau) e^{-i\pi \frac{\phi_k''(t)}{\phi_k'^2(t)}\eta^2\tau^2}\}(\eta)\right| \leq N_{r,p}\varepsilon$ when $|\eta - 1| > \Delta$, and $\int_{|\eta-1|>\Delta} \left|\mathcal{F}\{\psi(\tau) e^{-i\pi \frac{\phi_k''(t)}{\phi_k'^2(t)}\eta^2\tau^2}\}(\eta)\right| \frac{d\eta}{\eta} \leq N_2\widetilde{\varepsilon}$, for some constants $N_{r,p}$ and $N_2$.*

*Assuming $(t,a) \in \mathbb{E}$, then, provided $\varepsilon$ is sufficiently small, the following hold:*

*(a)* $|W_f^\psi(t,a)| > \widetilde{\varepsilon}$ *on* $\mathbb{E}$ *only when, there exists* $k \in \{1,\ldots,K\}$, *such that* $(t,a) \in Z_k := \{(t,a),\ s.t.\ |a\phi_k'(t) - 1| < \Delta\}$.

*(b) For each* $k \in \{1,\ldots,K\}$ *and for all* $(t,a) \in Z_k$, *for which hold* $|W_f^\psi(t,a)| > \widetilde{\varepsilon}$ *and* $|\partial_t \widetilde{\tau}_f(t,a)| > \widetilde{\varepsilon}$, *one has*

$$|\widehat{\omega}^{[2]}_{t,f}(t,a) - \phi_k'(t)| \leq \widetilde{\varepsilon}. \tag{26}$$

*(c) Moreover, for each* $k \in \{1,\ldots,K\}$, *there exists a constant* $D_2$ *such that*

$$\left|\left(\lim_{\lambda\to 0} \frac{1}{C'_{\psi,k}} \int_{|\omega-\phi_k'(t)|<\widetilde{\varepsilon}} S^{\lambda,\widetilde{\varepsilon}}_{2,W_f^\psi}(t,\omega)d\omega\right) - f_k(t)\right| \leq D_2\widetilde{\varepsilon}, \tag{27}$$

*with* $C'_{\psi,k} = \int_0^\infty \overline{\mathcal{F}\{\psi(\tau) e^{-i\pi \frac{\phi_k''(t)}{\phi_k'^2(t)}\eta^2\tau^2}\}(\eta)} \frac{d\eta}{\eta}$.

**Remark 3.** It is worth mentioning that the constant $C'_{\psi,k}$ involved in the reconstruction process depends on mode $k$ and is definitely different from $C'_\psi$ as soon as the modulation is non zero. Similarly, in the STFT context [21] [see Theorem 4]: the constant $g(0)$ in the reconstruction formula should actually be viewed as $\int_{\mathbb{R}} \overline{\mathcal{F}\{g(\tau)e^{-i\pi\phi_k''(t)\tau^2}\}(\eta)}d\eta$.

The proof of Theorem 2 is available in Section Appendix B.

## 5. Numerical Implementation of WSST2

This section details the numerical implementation of WSST2. The signal $f$ is assumed to be defined on $[0,1]$ and then uniformly discretized at time $t_m = m/n$ with $m = 0,\ldots,n-1$ and $n = 2^L$, $L \in \mathbb{N}$. First, we discretize $W_f^\psi$ at $(m/n, a_j)$, where $a_j = \frac{2^{j/n_v}}{n}$, $j = 0,\ldots,Ln_v$ with the "voice number" $n_v$ being a user-defined parameter controlling the number of scales ($n_v = 32$ or $64$ in practice). The Discrete Wavelet Transform (DWT) of $f$ is computed in the Fourier domain as follows:

$$W_f^\psi(t_m, a_j) \approx W^{\hat{\psi}}_{d,f}(m,j) := \left(\mathcal{F}_d^{-1}\left(\left(\mathcal{F}_d(f) \odot \overline{\hat{\psi}_{j,\cdot}}\right)\right)\right)_m, \tag{28}$$

where $\mathcal{F}_d(f)$ (*resp.* $\mathcal{F}_d^{-1}$) denotes the standard (*resp.* inverse) Discrete Fourier Transform (DFT) (*resp.* iDFT), $\odot$ the elementwise multiplication, and $\hat{\psi}_{j,q} = \hat{\psi}(a_j q)$ with $q = 0, \ldots, n-1$.

With this in mind, we compute the complex estimate of the second-order modulation operator $\widetilde{q}_{t,f}$ defined as in (23), as follows:

$$\widetilde{q}_{d,t,f}(m,j) = \frac{i2\pi \left( W_{d,f}^{\hat{\psi}}(m,j) W_{d,f}^{\xi^2\hat{\psi}}(m,j) - \left( W_{d,f}^{\xi\hat{\psi}}(m,j) \right)^2 \right)}{a_j^2 \left[ \left( W_{d,f}^{\hat{\psi}}(m,j) \right)^2 + W_{d,f}^{\hat{\psi}}(m,j) W_{d,f}^{\xi\hat{\psi}'}(m,j) - W_{d,f}^{\hat{\psi}'}(m,j) W_{d,f}^{\xi\hat{\psi}}(m,j) \right]},$$

where $W_{d,f}^{\xi^2\hat{\psi}}$, $W_{d,f}^{\xi\hat{\psi}}$, $W_{d,f}^{\xi\hat{\psi}'}$ , $W_{d,f}^{\hat{\psi}'}$ denote respectively DWTs of $f$ computed using the wavelets $\xi \mapsto \xi^2\hat{\psi}$, $\xi \mapsto \xi\hat{\psi}$, $\xi \mapsto \xi\hat{\psi}'$, and $\xi \mapsto \hat{\psi}'$. For instance $(\xi\hat{\psi})_{j,q} = (a_j q)\hat{\psi}(a_j q)$.

Introducing $\widetilde{\omega}_{d,f}(m,j) = \dfrac{W_{d,f}^{\xi\hat{\psi}}(m,j)}{a_j W_{d,f}^{\hat{\psi}}(m,j)}$ and $\widetilde{\tau}_{d,f}(m,j) = t + \dfrac{a_j}{i2\pi} \dfrac{W_{d,f}^{\hat{\psi}'}(m,j)}{W_{d,f}^{\hat{\psi}}(m,j)}$, enables the definition of a discrete version of a second-order complex IF estimate of $f$:

$$\widetilde{\omega}_{d,f}^{[2]}(m,j) = \begin{cases} \widetilde{\omega}_{d,f}(m,j) + \widetilde{q}_{d,t,f}(m,j)(t - \widetilde{\tau}_{d,f}(m,j)) & \text{if } \partial_t \widetilde{\tau}_{d,f}(m,j) \neq 0 \\ \widetilde{\omega}_{d,f}(m,j) & \text{otherwise,} \end{cases}$$

where $\partial_t \widetilde{\tau}_{d,f}(m,j) = \dfrac{\left( W_{d,f}^{\hat{\psi}}(m,j) \right)^2 + W_{d,f}^{\hat{\psi}}(m,j) W_{d,f}^{\xi\hat{\psi}'}(m,j) - W_{d,f}^{\hat{\psi}'}(m,j) W_{d,f}^{\xi\hat{\psi}}(m,j)}{W_{d,f}^{\hat{\psi}}(m,j)^2}$. We then take the real part $\widehat{\omega}_{d,f}^{[2]}(m,j) = \Re\{\widetilde{\omega}_{d,f}^{[2]}(m,j)\}$, which leads to the desired discrete IF estimate.

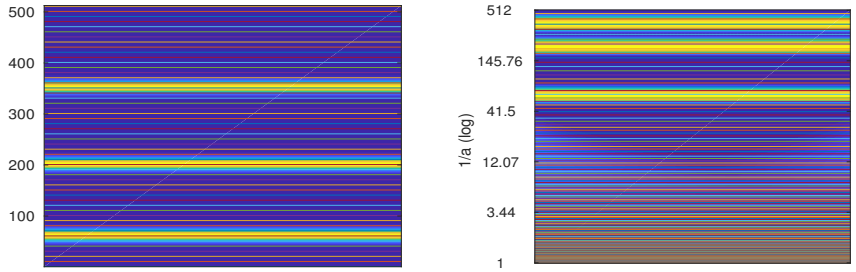


(a) (b)

Figure 1: (a), (b): modulus of STFT and WT of three constant frequency modes $f_1$, $f_2$, and $f_3$, with lines corresponding to the frequencies where the transforms are actually computed (linear scale for STFT and exponential one for WT).

We now show how to compute compute WSST2. First, we highlight how the frequency domain is split when performing second order synchrosqueezing

transform. First we remark that each scale $a_j$ is the inverse of frequency $f_j = 1/a_j = 2^{-j/n_v}n$. Putting $f_{Ln_v} = 0$ and $f_{-1} = +\infty$, we define frequency bins corresponding to the wavelet representation as $\mathcal{W}_j = \left[\frac{f_{j+1}+f_j}{2}, \frac{f_j+f_{j-1}}{2}\right[$, where $0 \leq j \leq Ln_v - 1$. With this in mind, the second order synchrosqueezing operator is implemented as follows:

$$S^{\gamma}_{d,2,f}(m/n, f_j) = \sum_{\mathbb{G}_d(j)} W^{\hat{\psi}}_{d,f}(m,l)\frac{\log(2)}{n_v}, \tag{29}$$

where $\mathbb{G}_d(j) = \left\{0 \leq l \leq Ln_v - 1 \text{ s.t. } \widehat{\omega}^{[2]}_{d,f}(m,l) \in \mathcal{W}_j \text{ and } |W^{\hat{\psi}}_{d,f}(m,l)| > \gamma\right\}$.

Finally, each mode $f_k$ is retrieved by summing $S^{\gamma}_{d,2,f}$ along the frequency axis in the vicinity of the $k$th mode. More precisely, one has, for each $t_m$,

$$f_k(m/n) \approx \frac{1}{C'_{d,\psi,k}} \sum_{l \in \Upsilon_k(m)} S^{\gamma}_{d,2,f}(m, \omega_l), \tag{30}$$

where $\Upsilon_k(m)$ is a set of indices corresponding to a small frequency band located around the ridge curve of $k$th mode, which is selected by ridge extraction method [23, 24], and $C'_{d,\psi,k}$ is a discrete approximation of $C'_{\psi,k}$.

**Remark 4.** It is important to remark here that the set $\Upsilon_k(m)$ is computed via ridge extraction on the wavelet representation, so that the accuracy of the reconstruction of the mode depends on the frequency band the mode leaves in. Indeed the size of $\mathcal{W}_{j-1}$ is $2^{1/n_v}$ the size of $\mathcal{W}_j$, meaning the accuracy of the set $\Upsilon_k(m)$ depends on the frequency of mode $k$. On the contrary, this is not the case when considering a synchrosqueezing operator based on STFT, for which one uses a uniform sampling of the frequency axis. With STFT, the length of the frequency bins is 1, while the length of $\mathcal{W}_j$ is smaller than 1 for large $j$ and much bigger for small ones. This is illustrated in Figure 1, where we consider three constant frequency modes: on that figure, we draw a line at each frequency used in the computation of CWT and STFT (along with the transforms themselves). We notice that while the error associated with IF estimation by ridge extraction is bounded by 1 for STFT, it depends on the frequency for CWT (the average IF estimation error associated with ridge extraction ranges from 0.55, 1.74 and 3.34 for $f_1$, $f_2$ and $f_3$ respectively) .

## 6. Numerical analysis of the behavior of WSST2 and comparisons

In this section, we provide numerical experiments to demonstrate the efficiency of our new transform WSST2 compared with other existing synchrosqueezing transforms including WSST, FSST, and FSST2 [21, 24, 27]. More precisely, we carry out a comparison in terms of concentration and accuracy of the TF representations obtained. For that purpose, we start with considering a complex

simulated MCS ($f$) composed of three components: a linear chirp ($f_1$), an hyperbolic chirp ($f_2$) and an exponential chirp ($f_3$) with Gaussian modulated amplitudes, whose instantaneous frequencies are respectively linear ($\phi''(t) \propto cst$), hyperbolic ($\phi''(t) \propto \phi'(t)^2$) and exponential ($\phi''(t) \propto \phi'(t)$). Note also that $f_1$ behaves locally as a Gaussian modulated linear chirp that is mathematically proved to be perfectly handled by both FSST2 and WSST2, while the other two components contain strong nonlinear frequency modulations.

In our simulations, $f$ is uniformly sampled over time interval $[0, 1]$ with a sampling rate $M = 1024$ Hz. An arbitrary threshold $\gamma = \gamma_0 = 0.001$ is set for noise-free signals (the results obtained relatively insensitive to that threshold). Also, we use the complex Morlet wavelet (*resp.* Gaussian window) to compute the CWT (*resp.* STFT), which depends on a parameter $\sigma_W = 5$ (*resp.* $\sigma_F = 0.05$) (these values are optimally selected by the Renyi entropy method [24]):

$$\psi(t, \sigma_W) = \frac{1}{\sqrt{\sigma_W}} e^{-\pi \frac{t^2}{\sigma_W^2}} e^{i2\pi t} \text{ and } g(t, \sigma_F) = \sigma_F^{-\frac{1}{2}} e^{-\pi \frac{t^2}{\sigma_F^2}}.$$

In addition, the wavelet-based (*resp.* STFT-based) synchrosqueezing transforms are represented on a logarithmic (*resp.* linear) scale. The Matlab codes for synchrosqueezing transforms and the scripts leading to all figures of this paper can be found https://github.com/phamduonghung/WSST2.

In Figures 2 (a), (b) and (c), we display respectively the real part of the three components along with their amplitudes, and, in Figure 2 (d), the real part of the whole signal.

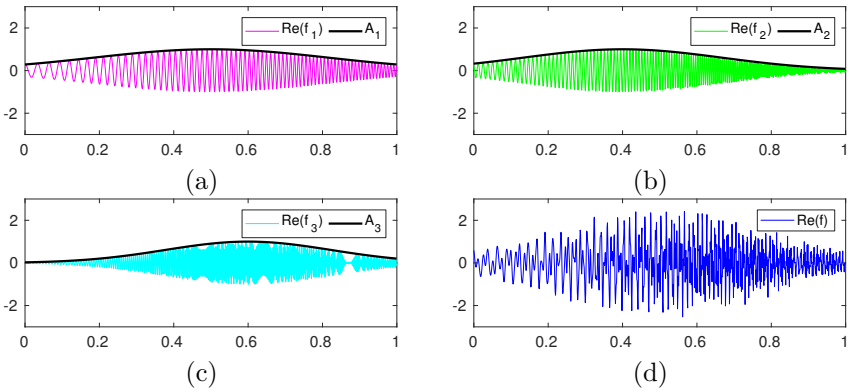


Figure 2: (a), (b) and (c): real part of $f_1$, $f_2$, and $f_3$ respectively with Gaussian modulated amplitudes $A_1$, $A_2$ and $A_3$ superimposed; (d): real part of $f$.

We then display, still in the noise-free context, the STFT and CWT of $f$ in the first column of Figure 3. Then, on the other two columns of this figure, the reassigned versions of CWT and STFT given by the aforementioned synchrosqueezing transforms are depicted.

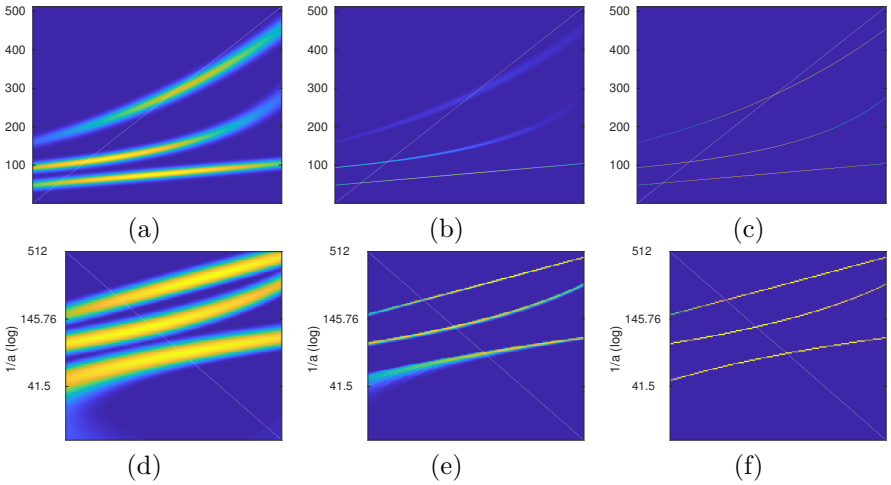


Figure 3: *First row*, (a): modulus of the STFT of $f$; (b): FSST; (c): FSST2 ; *Second row*, (d): modulus of the CWT of $f$; (e): WSST; (f) WSST2. Threshold $\gamma_0 = 0.001$.

Analyzing these figures, we first remark that, as expected, FSST leads to a relatively sharp TF representation for the linear chirp $f_1$, that looks similar to the ones given by WSST2 and FSST2, and much better than that corresponding to WSST. It is worth mentioning here that this worse representation is related to the scale discretization and not to the quality of the IF estimate as will be shown latter. We shall also remark that FSST fails to reassign correctly the STFT of $f_2$ and $f_3$ where their frequency modulations are non-negligible. In contrast, the reassigned representations of $f_2$ and $f_3$ provided by WSST are much more concentrated at these locations. Moreover, it is also of interest to remark that the quality of the representation corresponding to WSST seems not to depend on the scale for $f_2$ contrary to what happens with $f_3$. Finally, for $f_2$ and $f_3$, both WSST2 and FSST2 seem to behave very similarly when considering either of the three studied modes, and result in compact TF representations. We first study the stability of IF estimation with FSST and WSST on a linear chirp and then switch to that of WSST on an hyperbolic chirp.

### *6.1. Stability of IF estimation with FSST and WSST on a linear chirp*

To explain the different behaviors of STFT and WSST when applied to a linear chirp, we introduce some materials regarding regarding STFT, and the IF estimator used by FSST. STFT is defined by:

$$V_f^g(t,\eta) \quad = \int_{\mathbb{R}} f(\tau) g(\tau - t) e^{-2i\pi\eta(\tau - t)} d\tau, \tag{31}$$

and the instantaneous frequency estimator used in FSST, by

$$\widehat{\omega}_{f,F}(t,\eta) \quad = \quad \Re\left\{ \frac{1}{i2\pi} \frac{\partial_t V_f^g(\eta,t)}{V_f^g(\eta,t)} \right\}. \tag{32}$$

Note that we add a subscript $F$ in the definition of this estimator to mean that it is related to the Fourier transform. With this in mind, we introduce the linear chirp $h_c(t) = Ae^{2i\pi\phi(t)}$. It was proven in [21] that if $|\eta - \phi^{'}(t)| < \Delta$ then, when STFT is performed with $g_{\sigma_F}(t, \sigma_F)$ that

$$|\widehat{\omega}_{h_c,F}(t,\eta) - \phi^{'}(t)| \leq \quad \Delta \left|1 - \tfrac{1}{1+\sigma_F^4 \phi^{''}(t)^2}\right| \leq \Delta, \tag{33}$$

which means that this IF estimation is stable for all $t$.

Similarly, we study the quality of the estimate $\widehat{\omega}_{h_c}(t,a)$, for which we have the following result:

**Theorem 3.** *If one performs the decomposition with the Morlet wavelet $\psi(t, \sigma_W)$ if $|\frac{1}{a} - \phi^{'}(t)| \leq \Delta$ then:*

$$|\widehat{\omega}_{h_c}(t,a) - \phi^{'}(t)| \quad \leq \Delta, \tag{34}$$

*meaning the IF estimation is stable for all $t$.*

*Proof.* In such a case, one has, using a second order Taylor expansion of the phase of $h_c$:

$$\begin{aligned}
W_{h_c}^{\psi}(t,a) &= \int_{\mathbb{R}} Ae^{2i\pi\phi(\tau)} \sigma_W^{-1} e^{-\frac{\pi}{\sigma_W^2}\left(\frac{\tau-t}{a}\right)^2} e^{-2i\pi\left(\frac{\tau-t}{a}\right)} d\tau \\
&= h_c(t) a \sigma_W^{-1} \mathcal{F}\left\{ e^{-\pi\left[\frac{1}{\sigma_W^2} - ia^2\phi^{''}(t)\right]u^2} \right\} (1 - a\phi'(t)) \\
&= h_c(t) a \sigma_W^{-1} \left( \frac{1}{\sigma_W^2} - ia^2\phi^{''}(t) \right)^{-\frac{1}{2}} e^{\left[\frac{-\pi\sigma_W^2(1-a\phi^{'}(t))^2}{1-i\sigma_W^2 a^2 \phi^{''}(t)}\right]}.
\end{aligned}$$

With that expression, one can compute the estimate, bearing in mind that $\phi''(t)$ is constant and $\Im(z)$ is the imaginary part of complex number $z$:

$$\begin{aligned}
\widehat{\omega}_{h_c}(t,a) &= \Re\left\{ \frac{1}{i2\pi} \frac{\partial_t W_{h_c}^{\psi}(t,a)}{W_{h_c}^{\psi}(a,t)} \right\} = \frac{1}{2\pi} \Im\left\{ \frac{\partial_t W_{h_c}^{\psi}(t,a)}{W_{h_c}^{\psi}(t,a)} \right\} \\
&= \frac{1}{2\pi} \Im\left\{ \frac{h_c^{'}(t)}{h_c(t)} + \frac{2\pi\sigma_W^2 a \phi^{''}(t)(1 - a\phi^{'}(t))}{1 - i\sigma_W^2 a^2 \phi^{''}(t)} \right\} \\
&= \frac{1}{2\pi} \Im\left\{ 2i\pi\phi^{'}(t) \right\} + \left( \frac{\sigma_W^2 a \phi^{''}(t)(1 - a\phi^{'}(t))}{1 + \sigma_W^4 a^4 \phi^{''}(t)^2} (\sigma_W^2 a^2 \phi^{''}(t)) \right).
\end{aligned}$$

From this one derives:

$$\Rightarrow |\widehat{\omega}_{h_c}(t,a) - \phi^{'}(t)| = \left| \frac{\sigma_W^4 a^4 \phi^{''}(t)^2 \left(\frac{1}{a} - \phi^{'}(t)\right)}{1 + \sigma_W^4 a^4 \phi^{''}(t)^2} \right|.$$

If $|\frac{1}{a} - \phi^{'}(t)| \leq \Delta$ then $|\widehat{\omega}_{h_c}(t,a) - \phi^{'}(t)| \leq \Delta \left|1 - \frac{1}{1+\sigma_W^4 a^4 \phi^{''}(t)^2}\right| \leq \Delta.$ □

*6.2. Stability of IF estimation with WSST on a hyperbolic chirp*

In this section, we show that WSST is well behaved when applied to an hyperbolic chirp, as suggested by Figure 3 (e). We show, in the following theorem, the stability of IF estimation with $\hat{\omega}_f(t,a)$, when a Cauchy wavelet is used for the decomposition (the proof for the Morlet wavelet still needs to be carried out).

**Theorem 4.** *Let $f$ be an hyperbolic chirp defined by $f(t) = t^{i\alpha}$ for $0 < t$ and any $\alpha$ in $\mathbb{R}$, and consider the estimate $\widehat{\omega}_f(t,a)$ computed using the Cauchy wavelet with parameter 1. Then, if $|\frac{1}{a} - \phi^{'}(t)| \leq \Delta$, we have*

$$|\widehat{\omega}_f(t,a) - \phi^{'}(t)| \quad \leq \Delta. \tag{35}$$

*Proof.* First, let us recall the definition of the Cauchy wavelet of order $\beta$, a strictly positive real,

$$g_\beta(t) = \Gamma(\beta+1)(1 - i2\pi t)^{-(1+\beta)}, \tag{36}$$

where for any complex $z$ with strictly positive real part, $\Gamma(z) = \int_0^{+\infty} t^{z-1}e^{-t}dt$.

Note that when $\beta$ is an integer, $g_\beta$ admits the following Fourier transform $\hat{g}_\beta(\eta) = \eta^\beta e^{-\eta}H(\eta)$ with $H$ the Heaviside function. So, even if $\hat{g}_\beta$ is not compactly supported, it has a fast decay (the behavior of $\hat{g}_\beta$ being similar for non integer $\beta$).

First, let us first consider $f(t) = t^\alpha H(t)$, for any $\alpha > -1$ and let us compute its wavelet transform with the Cauchy wavelet with $\beta > \alpha$:

$$\begin{aligned}
W_f^{g_\beta}(t,a) = & \quad \tfrac{1}{a}\int_0^\infty \tau^\alpha \overline{g_\beta\left(\frac{\tau - t}{a}\right)}d\tau \\
= & \quad a^\beta\Gamma(\beta+1)\int_0^\infty \tau^\alpha \frac{1}{(a + i2\pi(\tau - t))^{-(1+\beta)}}d\tau \\
= & \quad a^\beta\Gamma(\beta+1)\int_0^\infty \tau^\alpha \left(\frac{-i}{(-2\pi t - ia) + 2\pi\tau}\right)^{1+\beta} d\tau \\
= & \quad a^\beta\Gamma(\beta+1)\int_0^\infty \tau^\alpha \left(\frac{-i}{z + 2\pi\tau}\right)^{1+\beta} d\tau,
\end{aligned}$$

with $z = -2\pi t - ia$, so that the wavelet transform can be viewed as analytic function in $z$.

Now, assuming $z$ is a positive integer, one can rewrite the wavelet transform, making the appropriate change of variable, as:

$$\begin{aligned}
W_f^{g_\beta}(t,a) &= (2\pi)^{-\alpha-1}a^\beta\Gamma(\beta+1)(-i)^{1+\beta}z^{\alpha-\beta}\int_0^\infty \tau^\alpha\left(\frac{1}{1+\tau}\right)^{1+\beta}d\tau \\
&= (2\pi)^{-\alpha-1}a^\beta\Gamma(\beta+1)(-i)^{1+\beta}z^{\alpha-\beta}B(\alpha+1,\beta-\alpha) \\
&= (2\pi)^{-\alpha-1}a^\beta\Gamma(\beta+1)B(\alpha+1,\beta-\alpha)e^{-i\pi\frac{1+\beta}{2}}z^{\alpha-\beta},
\end{aligned}$$

where $B$ is the beta function. The expression is then also true when $z$ is complex using the analytic continuation theorem.

Now using the analytic continuation theorem with variable $\alpha$ we have for the hyperbolic chirp $f(t) = t^{i\alpha}H(t)$, $\alpha \in \mathbb{R}$:

$$\begin{aligned} W_f^{g_\beta}(t,a) = & \quad (2\pi)^{-i\alpha-1}a^\beta\Gamma(\beta+1)B(i\alpha+1,\beta-i\alpha)e^{-i\pi\frac{1+\beta}{2}}z^{i\alpha-\beta}, \\ = & \quad (2\pi)^{-i\alpha-1}a^\beta\Gamma(\beta+1)B(i\alpha+1,\beta-i\alpha)e^{-i\pi\frac{1+\beta}{2}}(-2\pi t-ia)^{i\alpha-\beta}. \end{aligned}$$

Note that this expression is valid for any positive $\beta$, regardless of $\alpha$

Using that expression for the wavelet transform, we may then write:

$$\hat{\omega}_f(t,a) = \frac{1}{2\pi}\mathcal{I}\left[\frac{\partial_t W_f^{g_\beta}(t,a)}{W_f^{g_\beta}(t,a)}\right] = \mathcal{I}\left[-(i\alpha-\beta)(2\pi t+ia)^{-1}\right] = \frac{\alpha 2\pi t + a\beta}{a^2+4\pi^2t^2}$$

Thus one can deduce: $\left|\widehat{\omega}_f(t,a) - \frac{\alpha}{2\pi t}\right| = |\widehat{\omega}_f(a,t) - \phi'(t)| = \left|\frac{\frac{\beta}{a}-\frac{\alpha}{2\pi t}}{1+4\pi^2(\frac{t}{a})^2}\right|$.
Finally, if $|\frac{1}{a} - \phi^{'}(t)| \leq \Delta$ and $\beta = 1$: $|\widehat{\omega}_f(t,a) - \phi'(t)| \leq \frac{\Delta}{1+4\pi^2(\frac{t}{a})^2} \leq \Delta$. □

### *6.3. Evaluation of TF concentration*

The TF concentration is one of the outstanding features used for evaluating the performance of the different TF techniques. To quantify this, an appealing method first introduced in [27] and then applied successfully in [24] is used in this paper. The main aim of such a method is to measure the energy concentration by considering the proportion of the latter contained in the first nonzero coefficients associated with the highest amplitudes, which we call *normalized energy*. When computed on a mono-component signal, the faster it increases towards 1 with the number of coefficients involved, the more concentrated the TF representation. In Figure 4 (a), we depict the normalized energy corresponding to the reassignment of the STFT of $f_1$ using different techniques, with respect to the number of coefficients kept divided by the length of $f_1$ (which corresponds to the sampling rate $M$ in our case). Not surprisingly, the energy of $f_1$ is perfectly localized when using either WSST2 or FSST2, since they require only one coefficient per time instant to recover the signal energy, while WSST and FSST need more coefficients (5 and 2 respectively). The same computations carried out on $f_2$ and $f_3$ show that WSST2 still better performs than the other three methods, especially WSST or FSST.

To further challenge the different TF reassigned techniques in the presence of noise, we consider a noisy signal $f_\zeta(t) = f(t) + \zeta(t)$, where $\zeta(t)$ is a complex white Gaussian process with variance $\mathrm{Var}\left(\Re\left\{\zeta(t)\right\}\right) = \mathrm{Var}\left(\Im\left\{\zeta(t)\right\}\right) = \sigma_\zeta^2$. Furthermore, the noise level is measured by the Signal-to-Noise Ratio (SNR):

$$\mathrm{SNR}_{\mathrm{intput}}[\mathrm{dB}] = 20\log_{10}\frac{\|f\|_2}{\|f_\zeta - f\|_2}, \tag{37}$$

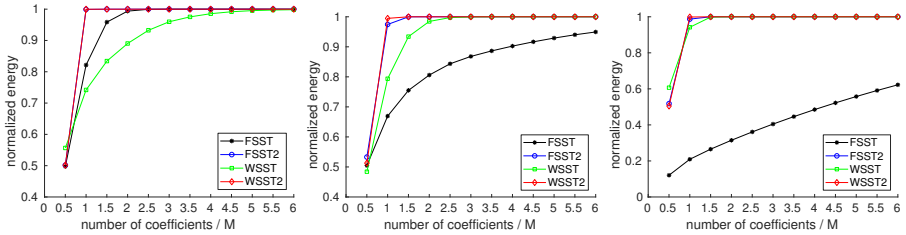


(a) (b) (c)

Figure 4: (a) Normalized energy as a function of the number of sorted TF coefficients for $f_1$. Abscissa corresponds to the number of coefficients over the size $M$ of the signal; (b): same as (a) but for $f_2$ ; (c): same as (a) but for $f_3$. Threshold $\gamma_0 = 0.001$.

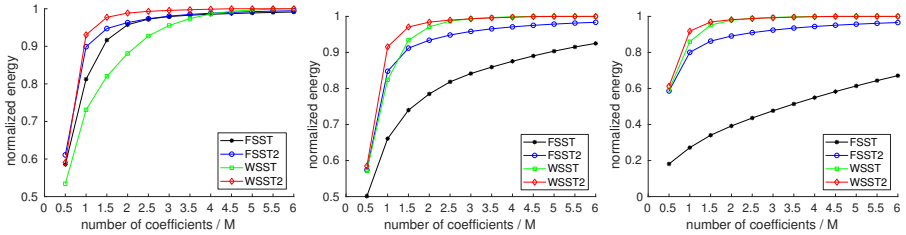


(a) (b) (c)

Figure 5: (a) Normalized energy as a function of the number of sorted TF coefficients for noisy $f_1$ (SNR= 0dB); (b): same as (a) but for noisy $f_2$ (at level 0dB); (c): same as (a) but for noisy $f_3$ (at level 0dB).

where $\|.\|_2$ is the $l_2$ norm. Note also that, in this noisy context, one of the well-known issue regarding the use of SST is the choice of an appropriate threshold $\gamma$ on $W_f^\psi(t,a)$ or $V_f^g(t,\eta)$ in the definition of the synchrosqueezing operator to allow for signal denoising and a fair comparison between the different tested methods. Here, we propose a technique enabling adaptive determination of the threshold $\gamma$ as a function of the noise level. Such a technique exploits the linearity of CWT and the fact that, for a fixed scale $a$, one has:

$$\text{std}\left(\Re\left\{W_\zeta^\psi(t,a)\right\}\right) = \sigma_\zeta \frac{1}{\sqrt{a}} \|\psi\|_2 \text{ and std}\left(\Im\left\{W_\zeta^\psi(t,a)\right\}\right) = \sigma_\zeta \frac{1}{\sqrt{a}} \|\psi\|_2 ,$$

where std is the standard deviation. Thus, if one chooses a threshold $\gamma_W = 3\sqrt{2}\sigma_\zeta \frac{1}{\sqrt{a}} \|\psi\|_2$ for CWT, keeping only the coefficients satisfying: $\left|W_{f_\zeta}^\psi(t,a)\right| > \gamma_W$ in the wavelet-based synchrosqueezing transforms guarantees an efficient noise removal. Note that the normalization factor $\sqrt{2}$ is used because we threshold the modulus of CWT rather than its real or imaginary parts. The same arguments apply to STFT by keeping only the coefficients such that $\left|V_{f_\zeta}^g(t,\eta)\right| > \gamma_F = 3\sqrt{2}\sigma_\zeta \|g\|_2$. In real-life applications, threshold level $\gamma_W$ and $\gamma_F$ are unknown and need to be estimated. For example, a robust estimator is

proposed in [28]:

$$\hat{\gamma}_W = \frac{\underset{a}{\text{median}} \left| \Re \left\{ W^{\psi}_{f_\zeta}(t,a) \right\} \right|}{0.6745} \text{ and } \hat{\gamma}_F = \frac{\underset{\eta}{\text{median}} \left| \Re \left\{ V^{g}_{f_\zeta}(t,\eta) \right\} \right|}{0.6745},$$

where median represents the median of the coefficients.

Using the just defined thresholds, we carry out the same numerical experiments regarding energy concentration as in the noise-free case, each mode being this time contaminated by a white Gaussian noise (SNR = 0dB). The results displayed in Figure 5 exhibit a slightly slower growth of the normalized energy since the coefficients corresponding to noise, that the above technique cannot completely eliminate, are spread out over the whole TF or TS planes. However, the normalized energy is still more concentrated when using WSST2 than the other methods, even for mode $f_1$ when compared with FSST2. These facts clearly show that the representation provided by the former technique is the most concentrated, even in heavy noise situations.

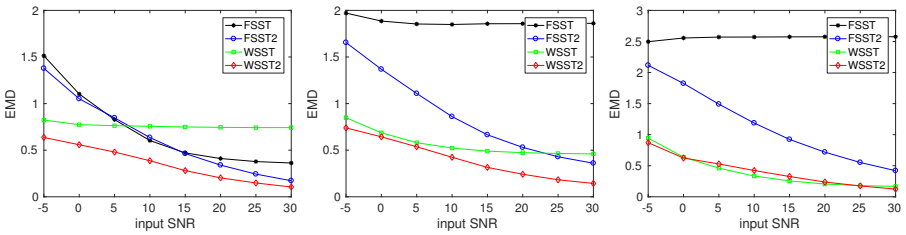


Figure 6: (a): EMD corresponding to different TF representations of $f_1$ given by the synchrosqueezing transforms; (b): same as (a) but for $f_2$; (c): same as (a) but for $f_3$.

Although quite informative, the method based on normalized energy does not deliver any insight into the location accuracy of the reassigned transforms. The latter can alternatively be quantified by measuring the dissimilarity between the resultant TF representations and the ideal one by means of the Earth mover's distance (EMD), a procedure already used in the synchrosqueezing context in [15]. The EMD is a sliced Wasserstein distance, commonly used in optimal transport, which allows for the comparison of two probability distributions. More precisely, it consists in computing the 1D EMD between the resultant TF representations and the ideal one, for each individual time $t$, and then take the average over all $t$ to define the global EMD. A smaller EMD means a better TF representation concentration to the ground truth and less noise fluctuations. In Figures 6 (a), (b) and (c), we display, respectively for the three modes already tested, the evolution of EMD with respect to the noise level, for TF representations given either by WSST, WSST2, FSST or FSST2. For linear chirp $f_1$, WSST2 always achieves the best performance of the TF concentration to the ground truth whatever the input SNR, even compared with FSST2. Moving to $f_2$ and $f_3$, WSST2 performs similarly to WSST at high noise

level and is more accurate at low noise level, while it consistently outperforms FSST and FSST2. These results confirm the interest of using WSST2 on many different types of signals, even in the presence of heavy noise.

### *6.4. Evaluation of mode reconstruction performance*

Table 1: Accuracy of mode retrieval in the noise-free case

| | **FSST** | **FSST2** | **WSST** | **WSST2** |
|---|---|---|---|---|
| Mode $f_1$ | 8.77 | 29.4 | 4.57 | **50.3** |
| Mode $f_2$ | 2.64 | 18.4 | 8.12 | **22.9** |
| Mode $f_3$ | 0.646 | 18.1 | 14.6 | **30.4** |
| MCS $f$ | 3.18 | 20.0 | 7.11 | **27.2** |

Table 2: Accuracy of mode retrieval in the noisy case, (at noise level 0dB)

| | **FSST** | **FSST2** | **WSST** | **WSST2** |
|---|---|---|---|---|
| Mode $f_1$ | 4.46 | 6.01 | 3.76 | **6.65** |
| Mode $f_2$ | 2.62 | 4.84 | 4.58 | **6.00** |
| Mode $f_3$ | 0.46 | 3.07 | 3.06 | **3.41** |
| MCS $f$ | 2.38 | 4.59 | 3.80 | **5.34** |

As discussed above, the variants of second order SST proposed in this paper leading to significantly better TF representations, this should translate into better performance in terms of mode reconstruction. Let us first briefly recall that $f_k$ is retrieved from the TF representation of $f$ given by the WSST2 (other SSTs have the same mode retrieval procedure) through:

$$f_k(m/n) \approx \frac{1}{C'_{d,\psi,k}} S^{\gamma}_{d,2,f}(m, \varphi_k(m/n)), \tag{38}$$

where $\varphi_k(m/n)$ is the estimate of $\phi'_k(m/n)$ given by the ridge detector (see [23] for details on such a technique used in this paper). This means that we only use the information on the ridge to reconstruct the mode. For that purpose, we measure the output SNR, defined by $\mathrm{SNR}_{\mathrm{output}} = 20 \log_{10} \frac{\|f\|_2}{\|f_r - f\|_2}$, where $f_r$ is the reconstructed signal. In Table 1, we display this output SNR for modes $f_1$, $f_2$, $f_3$ and also for $f$, using either FSST, FSST2, WSST or WSST2 for mode reconstruction. Further, we carry out the same experiments, but each mode is embedded in a white Gaussian noise at a noise level 0dB. The resultant accuracies for such a reconstruction are displayed in Table 2. From these results, we can see that the improvement brought by using WSST2 is clear

and consistent with the previous study of the accuracy of the proposed new TF representations.

### *6.5. Application to Gravitational-wave Signal*

This section investigates an application of our new technique on the analysis of a transient gravitational-wave signal. Its first observation was made in September 2015 and was announced by the LIGO and Virgo collaborations in February 2016 [19], and was named **GW150914**. Such a signal, detected by the LIGO detector in Hanford Washington, closely matches the predictions of general relativity for a gravitational wave emanating from the inward spiral and merger of a pair of black holes and the subsequent "ringdown" of the single resulting black hole. In our simulations, we use a Gaussian window and the Morlet wavelet with respective optimal values $\sigma_F = 0.05$ and $\sigma_W = 1$. In Figure 7 (a) and (c), we depict the modulus of STFT and CWT of the gravitational wave signal, then in Figure 7 (b) and (d), we display the modulus of FSST2 and WSST2 along with the ridges extracted from these TF representations. We notice that while ridge extraction performed on FSST2 misses the "ringdown" effect, such is not the case with WSST2.

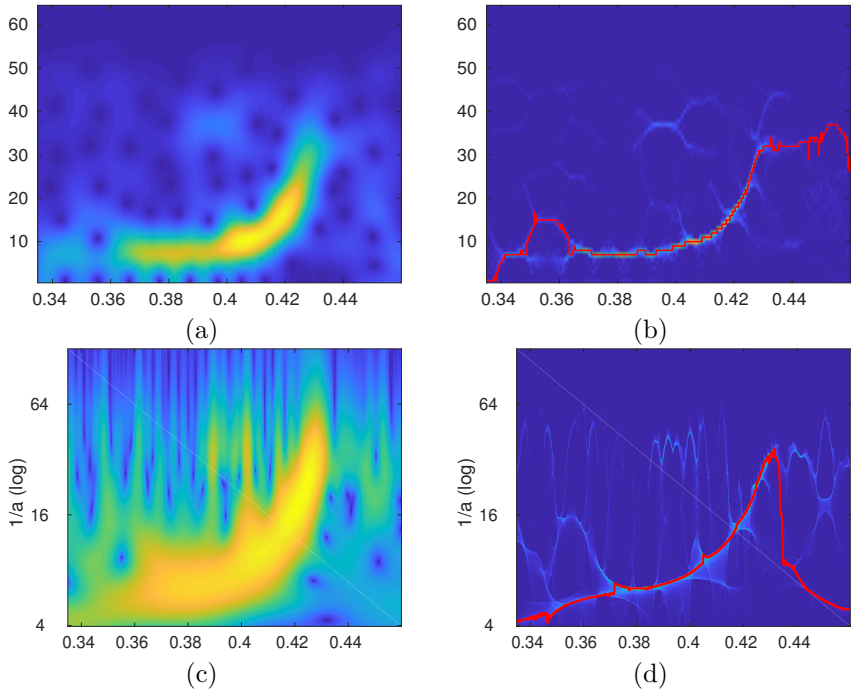


Figure 7: Illustration of the TF representations of the gravitational-wave event **GW150914**, (a): observed Hanford signal; (b): STFT; (c): FSST2; (d): WSST2.

## 7. Conclusion

This paper introduced a novel synchrosqueezing transform for analyzing multicomponent signals made of strongly frequency-modulated modes, based on the continuous wavelet transform. It simply consists of a refinement of the instantaneous frequency estimate, computed using a second-order expansion of the phase. After having revisited the case of first-order synchrosqueezing, releasing the hypothesis of a wavelet compactly supported in the frequency domain, we proved a novel approximation theorem involving the proposed new synchrosqueezing transform applied to multicomponent signals made of strongly modulated modes. In this regard we put forward a novel reconstruction technique for the modes. Numerical experiments showed the benefits of taking into account frequency modulation for both representation and reconstruction purposes, and also the better performance of second order reassignment based on wavelet compared to that based on STFT. Future work should now be devoted to the theoretical analysis of the behavior of the proposed representations when applied to noisy signals, as was done in [29, 30] for the original WSST. In this regard, it would also be of interest to study the behavior of the transform when the type of noise is non Gaussian.

## Appendix A1: Proof of Proposition 1

*Proof.* For each $k \in \{1, \dots, K\}$, a zeroth order Taylor expansion of the amplitude and first order expansion of the phase of $f_k$ leads to:

$$\begin{aligned} f_k(\tau) &= A_k(\tau) e^{i2\pi\phi_k(\tau)} \\ &= A_k(t) e^{i2\pi[\phi_k(t)+\phi_k'(t)(\tau-t)]} + (A_k(\tau) - A_k(t)) e^{i2\pi\phi_k(\tau)} \\ &\qquad + A_k(t)[e^{i2\pi[\phi_k(t)+\phi_k'(t)(\tau-t)+\int_t^\tau \phi_k''(x)(\tau-x)dx]} - e^{i2\pi[\phi_k(t)+\phi_k'(t)(\tau-t)]}] \\ &= f_{k,1}(\tau) + f_{k,2}(\tau) + f_{k,3}(\tau). \end{aligned}$$

Then, for any $(t, a)$, the first term can be written as:

$$W^{\psi}_{f_{k,1}}(t,a) = \frac{1}{a} A_k(t) e^{i2\pi\phi_k(t)} \int_{\mathbb{R}} e^{i2\pi\phi_k'(t)(\tau-t)} \overline{\psi\left(\frac{\tau-t}{a}\right)} d\tau = f_k(t) \overline{\widehat{\psi}(a\phi_k'(t))}.$$

The second term is bounded by:

$$\begin{aligned} \left|W^{\psi}_{f_{k,2}}(t,a)\right| &\leq \frac{1}{a} \int_{\mathbb{R}} |A_k(\tau) - A_k(t)| \left|\psi\left(\frac{\tau-t}{a}\right)\right| d\tau \\ &\leq \frac{\varepsilon M}{a} \int_{\mathbb{R}} |\tau - t| \left|\psi\left(\frac{\tau-t}{a}\right)\right| d\tau = \varepsilon a M J_{1,0}. \end{aligned}$$

and the third term by:

$$\left|W^{\psi}_{f_{k,3}}(t,a)\right| \leq \frac{2\pi A_k(t)}{a}\int_{\mathbb{R}}\left(\int_t^{\tau}|\phi_k''(u)||(\tau-u)|du\right)\left|\psi\left(\frac{\tau-t}{a}\right)\right|d\tau$$
$$\leq \frac{\varepsilon\pi M A_k(t)}{a}\int_{\mathbb{R}}|\tau-t|^2\left|\psi\left(\frac{\tau-t}{a}\right)\right|d\tau = \varepsilon\pi a^2 M J_{2,0}A_k(t).$$

Writing $|W^{\psi}_f - \sum_{k=1}^{K} W^{\psi}_{f_{k,1}}| = |\sum_{k=1}^{K}(W^{\psi}_{f_{k,2}} + W^{\psi}_{f_{k,3}})|$, we obtain the desired result. □

## Appendix B: Proof of Theorem 2

Theorem 2 is a generalization of Theorem 1, so the proof of the former is in principle similar to that of the latter. Proposition 1 generalizes into:

**Proposition 4.** *For any $k \in \{1,\dots,K\}$, any $r \in \{0,1\}$ and $p \in \{0,1\}$, and $(t,a) \in \mathbb{R}\times\mathbb{R}^+$, one has:*

$$\left|W_f^{\tau^r\psi^{(p)}(\tau)}(t,a) - \sum_{k=1}^{K} f_k(t)\overline{\mathcal{F}\{\tau^r\psi^{(p)}(\tau)e^{-i\pi\phi_k''(t)a^2\tau^2}\}(a\phi_k'(t))}\right| \leq \varepsilon E_{r,p}(t,a), \tag{39}$$

*with* $E_{r,p}(t,a) = a^{r+1}MKJ_{r+1,p} + \frac{\pi}{3}a^{r+3}MJ_{r+3,p}\sum_{k=1}^{K}A_k(t)$.

*Proof.* Following the same steps as the proof of Proposition 1, but using a zeroth order Taylor expansion of the amplitude and second order expansion of the phase of $f_k$, one has:

$$\begin{aligned}
f_k(\tau) &= A_k(\tau)e^{i2\pi\phi_k(\tau)}\\
&= A_k(t)e^{i2\pi[\phi_k(t)+\phi_k'(t)(\tau-t)+\frac{1}{2}\phi_k''(t)(\tau-t)^2]} + (A_k(\tau)-A_k(t))e^{i2\pi\phi_k(\tau)}\\
&+ A_k(t)\Big[e^{i2\pi[\phi_k(t)+\phi_k'(t)(\tau-t)+\frac{1}{2}\phi_k''(t)(\tau-t)^2+\frac{1}{2}\int_t^{\tau}\phi_k'''(x)(\tau-x)^2dx]}\\
&\qquad\qquad - e^{i2\pi[\phi_k(t)+\phi_k'(t)(\tau-t)+\frac{1}{2}\phi_k''(t)(\tau-t)^2]}\Big]\\
&= f_{k,1}(\tau) + f_{k,2}(\tau) + f_{k,3}(\tau).
\end{aligned}$$

Then, for any $(t,a) \in \mathbb{R}\times\mathbb{R}^+$, one has:

$$W^{\tau^r\psi^{(p)}(\tau)}_{f_{k,1}}(t,a) = f_k(t)\overline{\mathcal{F}\{\tau^r\psi^{(p)}(\tau)e^{-i\pi\phi_k''(t)a^2\tau^2}\}(a\phi_k'(t))},$$
$$\left|W^{\tau^r\psi^{(p)}(\tau)}_{f_{k,2}}(t,a)\right| \leq \varepsilon a^{r+1}MJ_{r+1,p},$$

and

$$|W_{f_{k,3}}^{\tau^r\psi^{(p)}(\tau)}(t,a)| \leq \varepsilon \frac{\pi}{3} a^{r+3} M A_k(t) J_{r+3,p},$$

from which one easily gets the inequality (39). □

Item (a) follows from this proposition remarking that if $(t,a) \in \mathbb{E} \setminus \bigcup_{l=1}^{K} Z_l$:

$$|W_f^{\psi}(t,a)| \leq \varepsilon(E_{0,0}(t,a) + N_{0,0} \sum_{k=1}^{K} A_k(t)) \leq \widetilde{\varepsilon},$$

when $\widetilde{\varepsilon}$ is sufficiently small, i.e.:

$$\widetilde{\varepsilon} \leq \frac{1}{\sqrt{2}} \min \left( \| E_{0,0}(t,a) \|_{\infty,\mathbb{E}}^{-\frac{1}{2}}, \left\| N_{0,0} \sum_{k=1}^{K} A_k(t) \right\|_{\infty,\mathbb{E}}^{-\frac{1}{2}} \right) \tag{40}$$

because $E_{0,0}(t,a)$ is bounded on $\mathbb{E}$.

Now, to prove item (b) of Theorem 2, we remark that Proposition 4 rewrites for any $(t,a) \in \mathbb{R} \times \mathbb{R}^+$:

$$\left| W_f^{\tau^r\psi^{(p)}(\tau)}(t,a) - \sum_{k=1}^{K} W_{f_{k,1}}^{\tau^r\psi^{(p)}(\tau)}(t,a) \right| \leq \varepsilon E_{r,p}(t,a), \tag{41}$$

which rewrites when $r = 0$ using an integration by parts:

$$\left| W_f^{\psi^{(p)}}(t,a) + 2i\pi a \sum_{k=1}^{K} \left( a\phi_k''(t) W_{f_{k,1}}^{\tau\psi^{(p-1)}(\tau)}(t,a) + \phi_k'(t) W_{f_{k,1}}^{\psi^{(p-1)}}(t,a) \right) \right| \leq \varepsilon E_{0,p}(t,a). \tag{42}$$

From equation (41), we deduce that if $(t,a) \in Z_k$,

$$\left| W_f^{\tau^r\psi^{(p)}(\tau)}(t,a) - W_{f_{k,1}}^{\tau^r\psi^{(p)}(\tau)}(t,a) \right| \leq \varepsilon \left( E_{r,p}(t,a) + \sum_{l \neq k} A_l(t) N_{r,p} \right). \tag{43}$$

**Proposition 5.** *For any $(t,a) \in Z_k$ such that $|W_f^{\psi}(t,a)| > \widetilde{\varepsilon}$ and $|\partial_t \widetilde{\tau}_f(t,a)| > \widetilde{\varepsilon}$ one has:*

$$|\widetilde{q}_{t,f}(t,a) - \phi_k''(t)| \leq \widetilde{\varepsilon}. \tag{44}$$

*Proof.* For any $(t,a) \in Z_k$ one has, using (42) and (43):

$$
\begin{aligned}
&|\phi_k''(t) - \widetilde{q}_{t,f}(t,a)| \\
&= \left| \frac{1}{2\pi a^2} \frac{W_f^{\psi'} \left[ W_f^{\psi'} + i2\pi a (a\phi_k''(t) W_f^{t\psi} + \phi_k'(t) W_f^{\psi}) \right] - W_f^{\psi} \left[ W_f^{\psi''} + i2\pi a (a\phi_k''(t) W_f^{t\psi'} + \phi_k'(t) W_f^{\psi'}) \right]}{W_f^{t\psi} W_f^{\psi'} - W_f^{t\psi'} W_f^{\psi}} \right| \\
&\leq \left| \frac{1}{2\pi a^2} \frac{W_f^{\psi'} \left[ W_f^{\psi'} + i2\pi a (a\phi_k''(t) W_{f_{k,1}}^{t\psi} + \phi_k'(t) W_{f_{k,1}}^{\psi}) \right] - W_f^{\psi} \left[ W_f^{\psi''} + i2\pi a (a\phi_k''(t) W_{f_{k,1}}^{t\psi'} + \phi_k'(t) W_{f_{k,1}}^{\psi'}) \right]}{W_f^{t\psi} W_f^{\psi'} - W_f^{t\psi'} W_f^{\psi}} \right| \\
&+ \frac{1}{a} \frac{\left| a\phi_k''(t) W_f^{\psi'} (W_f^{t\psi} - W_{f_{k,1}}^{t\psi}) \right| + \phi_k'(t) \left| W_f^{\psi} - W_{f_{k,1}}^{\psi} \right| + \left| a\phi_k''(t) W_f^{\psi} (W_f^{t\psi'} - W_{f_{k,1}}^{t\psi'}) \right| + \phi_k'(t) \left| W_f^{\psi'} - W_{f_{k,1}}^{\psi'} \right|}{\left| W_f^{t\psi} W_f^{\psi'} - W_f^{t\psi'} W_f^{\psi} \right|} \\
&= \left| \frac{1}{2\pi a^2} \frac{W_f^{\psi'} (W_f^{\psi'} - W_{f_{k,1}}^{\psi'}) - W_f^{\psi} (W_f^{\psi''} - W_{f_{k,1}}^{\psi''})}{W_f^{t\psi} W_f^{\psi'} - W_f^{t\psi'} W_f^{\psi}} \right| \\
&+ \frac{1}{a} \frac{\left| a\phi_k''(t) W_f^{\psi'} (W_f^{t\psi} - W_{f_{k,1}}^{t\psi}) \right| + \phi_k'(t) \left| W_f^{\psi} - W_{f_{k,1}}^{\psi} \right| + \left| a\phi_k''(t) W_f^{\psi} (W_f^{t\psi'} - W_{f_{k,1}}^{t\psi'}) \right| + \phi_k'(t) \left| W_f^{\psi'} - W_{f_{k,1}}^{\psi'} \right|}{\left| W_f^{t\psi} W_f^{\psi'} - W_f^{t\psi'} W_f^{\psi} \right|} \\
&\leq \frac{\varepsilon \left( \left( \left| \frac{W_f^{\psi'}}{2\pi a^2} \right| + \left| \frac{\phi_k'(t)}{a} \right| \right) E_{0,1}(t,a) + \left| \frac{W_f^{\psi}}{2\pi a^2} \right| E_{0,2}(t,a)| + \left| \phi_k''(t) W_f^{\psi'} \right| E_{1,0}(t,a) + \frac{\phi_k'(t)}{a} E_{0,0}(t,a) + |\phi_k''(t)| E_{1,1}(t,a) \right)}{\left| W_f^{t\psi} W_f^{\psi'} - W_f^{t\psi'} W_f^{\psi} \right|} \\
&+ \varepsilon \frac{\sum_{l \neq k} A_l(t) \left( \left( \left| \frac{W_f^{\psi'}}{2\pi a^2} \right| + \left| \frac{\phi_k'(t)}{a} \right| \right) N_{0,1} + \left| \frac{W_f^{\psi}}{2\pi a^2} \right| N_{0,2}| + \left| \phi_k''(t) W_f^{\psi'} \right| N_{1,0} + \frac{\phi_k'(t)}{a} N_{0,0} + |\phi_k''(t)| N_{1,1} \right)}{\left| W_f^{t\psi} W_f^{\psi'} - W_f^{t\psi'} W_f^{\psi} \right|} \\
&\leq \frac{\varepsilon \left( \left( \left| \frac{W_f^{\psi'}}{2\pi a^2} \right| + \left| \frac{\phi_k'(t)}{a} \right| \right) E_{0,1}(t,a) + \left| \frac{W_f^{\psi}}{2\pi a^2} \right| E_{0,2}(t,a)| + \left| \phi_k''(t) W_f^{\psi'} \right| E_{1,0}(t,a) + \frac{\phi_k'(t)}{a} E_{0,0}(t,a) + |\phi_k''(t)| E_{1,1}(t,a) \right)}{\widetilde{\varepsilon}^3} \\
&+ \varepsilon \frac{\sum_{l \neq k} A_l(t) \left( \left( \left| \frac{W_f^{\psi'}}{2\pi a^2} \right| + \left| \frac{\phi_k'(t)}{a} \right| \right) N_{0,1} + \left| \frac{W_f^{\psi}}{2\pi a^2} \right| N_{0,2}| + \left| \phi_k''(t) W_f^{\psi'} \right| N_{1,0} + \frac{\phi_k'(t)}{a} N_{0,0} + |\phi_k''(t)| N_{1,1} \right)}{\widetilde{\varepsilon}^3} \leq \widetilde{\varepsilon},
\end{aligned}
$$

if $\widetilde{\varepsilon}$ is sufficiently small, the last inequality being obtained by remarking the numerator is bounded on $\mathbb{E}$. Note also, that $|\phi_k''(t) - \widetilde{q}_{t,f}(t,a)|$ is of the order of $\widetilde{\varepsilon}^3$ if $\varepsilon$ is sufficiently small. □

Proof of item (b): according to definition of $\widetilde{\omega}_{t,f}^{[2]}(t,a)$ in (21), one has:

$$\widetilde{\omega}_{t,f}^{[2]}(t,a) = \widetilde{\omega}_f(t,a) + \widetilde{q}_{t,f}(t,a)(t - \widetilde{\tau}_f(t,a)).$$

It follows that for $(t,a) \in Z_k$, such that $|W_f^\psi(t,a)| > \widetilde{\varepsilon}$ and $|\partial_t \widetilde{\tau}_f(t,a)| > \widetilde{\varepsilon}$

$$\begin{aligned}
&\left|\widetilde{\omega}_{t,f}^{[2]}(t,a) - \phi_k'(t)\right| \\
&\quad = \left| \frac{1}{i2\pi a} \frac{W_f^{\psi'}(t,a) + i2\pi a \phi_k'(t) W_f^\psi(t,a) + i2\pi a^2 \phi_k''(t) W_f^{t\psi}(t,a)}{W_f^\psi(t,a)} \right| \\
&\qquad\qquad + \left| a \frac{(\widetilde{q}_{t,f}(t,a) - \phi_k''(t))\, W_f^{t\psi}(t,a)}{W_f^\psi(t,a)} \right| \\
&\leq \frac{\frac{1}{2\pi a}\left|W_f^{\psi'}(t,a) - W_{f_{k,1}}^{\psi'}(t,a)\right| + \phi_k'(t)\left|W_f^\psi(t,a) - W_{f_{k,1}}^\psi(t,a)\right| + a\,|\phi_k''(t)|\left|W_f^{t\psi(t)}(t,a) - W_{f_{k,1}}^{t\psi(t)}(t,a)\right|}{W_f^\psi(t,a)} \\
&\qquad\qquad + \left| a \frac{(\widetilde{q}_{t,f}(t,a) - \phi_k''(t))\, W_f^{t\psi}(t,a)}{W_f^\psi(t,a)} \right| \\
&\leq \widetilde{\varepsilon}^5 \left( \frac{1}{2\pi a}(E_{0,1} + \sum_{l\neq k} A_l(t) N_{0,1}) \right) + \phi_k'(t) \left( E_{0,0} + \sum_{l\neq k} A_l(t) N_{0,0} \right) + a\,|\phi_k''(t)| \left( E_{0,1} + \sum_{l\neq k} A_l(t) N_{1,1} \right) \\
&\qquad\qquad + \left| a \frac{(\widetilde{q}_{t,f}(t,a) - \phi_k''(t))\, W_f^{t\psi}(t,a)}{\widetilde{\varepsilon}} \right| \leq \widetilde{\varepsilon}
\end{aligned}$$

when $\widetilde{\varepsilon}$ is sufficiently small.

Proof of item (c): It is exactly the same as in the weak modulation case (item (c) of Theorem 1), except that we use, at the very end of the proof, the following hypotheses:

$$\begin{aligned}
&\left| \lim_{\lambda\to 0} \left( \frac{1}{C'_{\psi,k}} \int_{|\omega - \phi_k'(t)| < \widetilde{\varepsilon}} S^{\lambda,\widetilde{\varepsilon}}_{2,W_f^\psi}(t,\omega) d\omega \right) - f_k(t) \right| = \left| \frac{1}{C'_{\psi,k}} \int_{\mathbb{X}} W_f^\psi(t,a) \frac{da}{a} - f_k(t) \right| \\
&\leq \left[ \left| \frac{1}{C'_{\psi,k}} \int_{|a\phi_k'(t)-1|<\Delta} W_f^\psi(t,a) \frac{da}{a} - f_k(t) \right| + \left| \frac{1}{C'_{\psi,k}} \int_{|W_f^\psi(t,a)| \leq \widetilde{\varepsilon} \cap |a\phi_k'(t)-1|<\Delta} W_f^\psi(t,a) \frac{da}{a} \right| \right] \\
&\leq \frac{1}{\left|C'_{\psi,k}\right|} \left[ \int_{|a\phi_k'(t)-1|<\Delta} \left| W_f^\psi(t,a) - f_k(t) \overline{\mathcal{F}\{\psi(\tau) e^{-i\pi\phi_k''(t)a^2\tau^2}\}(a\phi_k'(t))} \right| \frac{da}{a} + \right. \\
&\left. A_k(t) \int_{|a\phi_k'(t)-1|\geq\Delta} \left| \overline{\mathcal{F}\{\psi(\tau) e^{-i\pi\phi_k''(t)a^2\tau^2}\}(a\phi_k'(t))} \right| \frac{da}{a} + \widetilde{\varepsilon} \log\left(\frac{1+\Delta}{1-\Delta}\right) \right] \\
&\leq \frac{1}{\left|C'_{\psi,k}\right|} \left[ \varepsilon \int_{|a\phi_k'(t)-1|<\Delta} \left( E_{0,0}(t,a) + N_{0,0} \sum_{l\neq k} A_l(t) \right) \frac{da}{a} + + \widetilde{\varepsilon}(1 + A_k(t) N_2) \log\left(\frac{1+\Delta}{1-\Delta}\right) \right] \leq D_2 \widetilde{\varepsilon}.
\end{aligned}$$

## References


[1] I. Daubechies, J. Lu, and H.-T. Wu, "Synchrosqueezed wavelet transforms: an empirical mode decomposition-like tool," *Applied and Computational Harmonic Analysis*, vol. 30, no. 2, pp. 243–261, 2011.

[2] M. Costa, A. A. Priplata, L. A. Lipsitz, Z. Wu, N. E. Huang, A. L. Goldberger, and C.-K. Peng, "Noise and poise: Enhancement of postural complexity in the elderly with a stochastic-resonance-based therapy," *Europhysics Letters (EPL)*, vol. 77, no. 6, p. 68008, Mar 2007.

[3] D. A. Cummings, R. A. Irizarry, N. E. Huang, T. P. Endy, A. Nisalak, K. Ungchusak, and D. S. Burke, "Travelling waves in the occurrence of dengue haemorrhagic fever in Thailand," *Nature*, vol. 427, no. 6972, pp. 344 –347, Jan 2004.

[4] N. E. Huang and Z. Wu, "A review on Hilbert-huang transform: Method and its applications to geophysical studies," *Reviews of Geophysics*, vol. 46, no. 2, Jun 2008.

[5] Y. Y. Lin, H.-T. Wu, C. A. Hsu, P. C. Huang, Y. H. Huang, and Y. L. Lo, "Sleep apnea detection based on thoracic and abdominal movement signals of wearable piezo-electric bands," *IEEE Journal of Biomedical and Health Informatics*, 2016.

[6] C. L. Herry, M. Frasch, A. J. Seely, and H.-T. Wu, "Heart beat classification from single-lead ecg using the synchrosqueezing transform," *Physiological Measurement*, vol. 38, no. 2, pp. 171–187, 2017.

[7] S. Meignen, T. Oberlin, and S. McLaughlin, "A new algorithm for multicomponent signals analysis based on synchrosqueezing: With an application to signal sampling and denoising," *IEEE Transactions on Signal Processing*, vol. 60, no. 11, pp. 5787–5798, 2012.

[8] P. Flandrin, *Time-frequency/time-scale analysis*. Academic Press, 1998, vol. 10.

[9] K. Kodera, R. Gendrin, and C. Villedary, "Analysis of time-varying signals with small bt values," *IEEE Transactions on Acoustics, Speech, and Signal Processing*, vol. 26, no. 1, pp. 64–76, Feb 1978.

[10] F. Auger and P. Flandrin, "Improving the readability of time-frequency and time-scale representations by the reassignment method," *IEEE Transactions on Signal Processing*, vol. 43, no. 5, pp. 1068–1089, 1995.

[11] G. Thakur and H.-T. Wu, "Synchrosqueezing-based recovery of instantaneous frequency from nonuniform samples." *SIAM J. Math. Analysis*, vol. 43, no. 5, pp. 2078–2095, 2011.

[12] M. Clausel, T. Oberlin, and V. Perrier, "The monogenic synchrosqueezed wavelet transform: a tool for the decomposition/demodulation of am-fm images," *Applied and Computational Harmonic Analysis*, vol. 39, no. 3, pp. 450–486, Nov 2015.

[13] H. Yang and L. Ying, "Synchrosqueezed wave packet transform for 2D mode decomposition," *SIAM Journal on Imaging Sciences*, vol. 6, no. 4, pp. 1979–2009, Jan 2013.

[14] H. Yang, "Synchrosqueezed wave packet transforms and diffeomorphism based spectral analysis for 1d general mode decompositions," *Applied and Computational Harmonic Analysis*, vol. 39, no. 1, pp. 33–66, July 2015.

[15] I. Daubechies, Y. G. Wang, and H.-T. Wu, "Conceft: concentration of frequency and time via a multitapered synchrosqueezed transform," *Philosophical Transactions of the Royal Society A: Mathematical, Physical and Engineering Sciences*, vol. 374, no. 2065, Mar 2016.

[16] M. Skolnik, *Radar Handbook*, Technology and Engineering, Eds. McGraw-Hill Education, 2008.

[17] J. W. Pitton, L. E. Atlas, and P. J. Loughlin, "Applications of positive time-frequency distributions to speech processing," *IEEE Transactions on Speech and Audio Processing*, vol. 2, no. 4, pp. 554–566, 1994.

[18] E. J. Candes, P. R. Charlton, and H. Helgason, "Detecting highly oscillatory signals by chirplet path pursuit," *Applied and Computational Harmonic Analysis*, vol. 24, no. 1, pp. 14–40, 2008.

[19] B. P. Abbott and al., "Observation of gravitational waves from a binary black hole merger," *Phys. Rev. Lett.*, vol. 116, 2016.

[20] T. Oberlin, S. Meignen, and V. Perrier, "The fourier-based synchrosqueezing transform," in *2014 IEEE International Conference on Acoustics, Speech and Signal Processing (ICASSP)*, May 2014, pp. 315–319.

[21] R. Behera, S. Meignen, and T. Oberlin, "Theoretical analysis of the second-order synchrosqueezing transform," *Applied and Computational Harmonic Analysis*, Nov 2016.

[22] I. Daubechies and S. Maes, "A nonlinear squeezing of the continuous wavelet transform based on auditory nerve models," *Wavelets in medicine and biology*, pp. 527–546, 1996.

[23] R. Carmona, W. Hwang, and B. Torresani, "Characterization of signals by the ridges of their wavelet transforms," *IEEE Transactions on Signal Processing*, vol. 45, no. 10, pp. 2586–2590, Oct 1997.

[24] D.-H. Pham and S. Meignen, "High-order synchrosqueezing transform for multicomponent signals analysis - with an application to gravitational-wave signal," *IEEE Transactions on Signal Processing*, vol. 65, no. 12, pp. 3168–3178, June 2017.

[25] C. K. Chui, Y.-T. Lin, and H.-T. Wu, "Real-time dynamics acquisition from irregular samples — with application to anesthesia evaluation," *Analysis and Applications*, vol. 14, no. 04, pp. 537–590, jul 2016.

[26] T. Oberlin and S. Meignen, "The second-order wavelet synchrosqueezing transform," in *42th International Conference on Acoustics, Speech, and Signal Processing (ICASSP)*, 2017.

[27] T. Oberlin, S. Meignen, and V. Perrier, "Second-order synchrosqueezing transform or invertible reassignment? Towards ideal time-frequency representations," *IEEE Transactions on Signal Processing*, vol. 63, no. 5, pp. 1335–1344, March 2015.

[28] D. Donoho and I. Johnstone, "Ideal spatial adaptation via wavelet shrinkage," *Biometrika*, vol. 81, pp. 425–455, 1994.

[29] G. Thakur, E. Brevdo, N. S. FučKar, and H.-T. Wu, "The synchrosqueezing algorithm for time-varying spectral analysis: Robustness properties and new paleoclimate applications," *Signal Processing*, vol. 93, no. 5, pp. 1079–1094, May 2013.

[30] H. Yang, "Statistical analysis of synchrosqueezed transforms," *Applied and Computational Harmonic Analysis*, Jan. 2017.